UNIVERSAL BIREFRINGENT FILTER WITH A NEW DOUBLE PASSBAND MODE

JINGSHAN WANG, GUOXIANG AI, GUOFENG SONG, BIN ZHANG, XIANGMING YE and YINGPING NIE
Beijing Astronomical Observatory, Chinese Academy of Sciences, Beijing, 100080, China

and

TZIHONG CHIVEH, WEANSHUN TSAY and HUANSHIN LI
Department of Physics, National Central University, Chung-Li, Taiwan

(Received 23 September, 1994; in revised form 8 April, 1995)

Abstract. This article describes the universal birefringent filter (UBF) which will be mounted at Taiwan. The UBF permits observations of solar images, vector magnetic fields and/or line-of-sight velocity fields in any Fraunhofer line in the wavelength region from 4000 Å to 7000 Å with half width from 0.05 Å to 0.14 Å. We have tested it at ten Fraunhofer lines under a spectral telescope in Huairou Station of Beijing Astronomical Observatory and obtained the passband profiles. The principles of magnetic field and velocity field measurement with the UBF are also described.

1. Introduction

The birefringent filter is playing an important role in solar observations. Since the 1930's, there have been many types of birefringent filter developed, such as the Lyot type (Lyot, 1944), Evans type (Evans, 1949), Šolc type (Šolc, 1949), partially polarized filter (Title, 1976), multichannel birefringent filter (Ai and Hu, 1984). Most of the birefringent filters work at just one wavelength for observing one layer on the Sun. The universal birefringent filter uses achromatic waveplates and rotating polarizers to tune the passband rapidly, therefore one can measure the magnetic fields with magnetic sensitive lines and line-of-sight velocity field in a large spectral range (according to the achromatism of the waveplates) on the Sun. In this article, we describe the optical design, method of testing the filter and the measuring principles of the magnetic field and velocity field of the universal birefringent filter (UBF).

2. Optical System of the UBF

2.1. Optical Design

This UBF is designed on the principle of the Lyot-type birefringent filter (Figure 1). It contains seven crystal elements which are made of calcite with axes cut parallel to their optic axis. Five elements use the so-called wide-angle configuration in

Solar Physics **161:** 229–239, 1995.

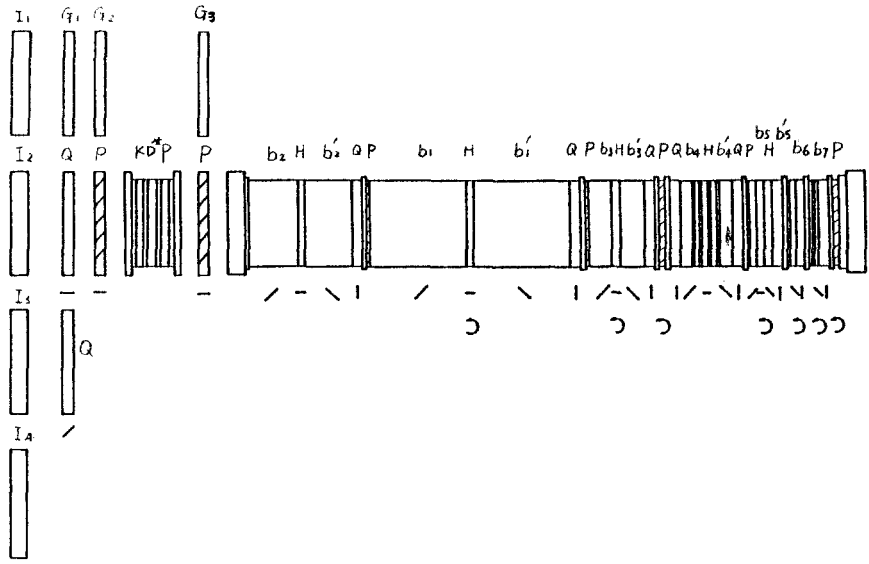

Fig. 1. Optical design diagram of the UBF. I_1-I_4: prefilter; Q: quarter achromatic waveplate; H: half achromatic waveplate; b_1-b_7: birefringent crystal element; P: polarizer; G_1-G_3: glass.

which each element is split into two equal parts with their optical axes crossed. The two equal parts are separated by a half waveplate with optical axis at 45° to that of the two halves. This half-wave plate has to be achromatic so that it has a 180° retardation at each wavelength. The other two are so-called narrow field elements. The parameters of the crystal elements are listed in Table I. In order to tune the passband wavelength, one can add to each element a quarter achromatic waveplate with its optical axis at 45° to the axis of the birefringent element and rotate the polarizer following this quarter waveplate. Figure 2 is a scheme of a tunable element in the UBF. Let σ be the phase difference of the crystal and ψ be the rotating angle of the following polarizer, then the transmissivity of this element is

$$\tau = \cos^2(\sigma/2 + \psi) \,. \tag{2.1}$$

Therefore the period of ψ is π. The tuning of the UBF is driven by seven independent step motors, and the step number of the motors corresponding to a circle of the rotated element is 15 120. Thus the step number of a period of ψ is 7560.

The relationship between the azimuth of the quarter waveplate near the element, rotating angle of polarizer and the passband shift is given in Table II (Wang, Ai, and Deng, 1991). It obeys a 'symbol multiply rule' (Table II). We control the step motors with a personal computer, and stipulate that the passband wavelength will increase (red shift) or decrease (violet shift) when the motors move positive

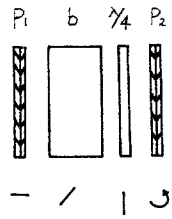

Fig. 2. A scheme of a tunable element.

TABLE I

The parameters of the optical components in the UBF

Component	Material	Thickness (mm)	Wide field or not	Optic orientation to side
The 1st element	Calcite	42.000 × 2	Yes	45°
The 2nd element	Calcite	21.000 × 2	Yes	45°
The 3rd element	Calcite	10.500 × 2	Yes	45°
The 4th element	Calcite	5.250 × 2	Yes	45°
The 5th element	Calcite	2.625 × 2	Yes	45°
The 6th element	Calcite	2.625	No	45°
The 7th element	Calcite	1.313	No	45°
Polarizer	HN42-HE	2.00	–	0°
Waveplate	PVA film	2.20	–	0°

or negative steps. This is very convenient for testing or shifting the passband of tunable birefringent filters.

Table III lists the properties of the UBF which include FWHM (full width at half-maximum) and the transmissivity at different spectral lines.

TABLE II

Relations between the pass-band tuning and the orientation arrangement of the crystal elements (the symbol-multiply rule)

ϕ between the $\lambda/4$ and the fast axis of the nearest crystal	Rotation angle θ of the rotating $\lambda/2$ retardation	Variation of the pass band	Tuned direction
+	+	+	Red shift
+	−	−	Violet shift
−	+	−	Violet shift
−	−	+	Red shift

TABLE III

The properties of the UBF

Wavelength (Å)	FWHM (Å)	Transmissivity[a]
6563.808	0.136	11.0%
6302.505	0.125	10.5%
6102.722	0.116	10.1%
5875.743	0.106	9.6%
5576.097	0.094	9.2%
5324.185	0.083	8.0%
5250.212	0.082	7.8%
5172.699	0.081	7.6%
4861.332	0.068	6.5%
4686.682	0.062	5.5%

[a] Excluding the prefilters.

TABLE IVa

The parameters of half PVA plastic achromatic waveplates

The designed central wavelength λ_0	The retardations and orientations of the individual plates of the half waveplate	The wavelength of the testing light	Region of retardation	The largest relative error
5600 Å	1. The retardations of the first and third plate are π (at λ_0), and the azimuth of their axis are all $-30°30'$;	6563 Å	0.4961–0.5056	1.12%
		5893 Å	0.4930–0.5052	−1.40%
	2. The retardation of the second plate is also π (at λ_0), the azimuth is $28°30'$	5461 Å	0.4923–0.5031	−1.54%
		4861 Å	0.4997–0.5090	1.80%

TABLE IVb

The parameters of quarter PVA plastic achromatic waveplates

The designed central wavelength λ_0	The retardations and orientations of the individual plates of the half waveplate	The wavelength of the testing light	Region of retardation	The largest relative error
5600 Å	1. The retardations of the first and third plate are 115°30 (at λ_0), and the azimuth of their axis are all $-30°45'$;	6563 Å	0.2435–0.2502	−2.56%
		5893 Å	0.2491–0.2573	2.92%
	2. The retardation of the second plate is π (at λ_0), the azimuth is $39°28'$	5461 Å	0.2499–0.2554	2.16%
		4861 Å	0.2449–0.2522	−2.40%

Let the phase differences of the birefringent elements be $\sigma_i = \mu d_i/\lambda$, $i = 1, 2, \ldots, 7$, and the rotating angles are ψ_i, $i = 1, 2, \ldots, 7$. If a horizontal polarizer is put in front of the second thickest element, we can get the transmissivity of the UBF:

$$\tau = \cos(\sigma_2/2 + \psi_1)\cos^2(\sigma_1/2 + \psi_2 - \psi_1)\ldots\cos^2(\sigma_7/2 + \psi_7 - \psi_6)\,. \quad (2.2)$$

2.2. HIGH-QUALITY PVA ACHROMATIC WAVEPLATE

We used Panchatnam's type achromatic waveplate (Panchatnam, 1955a, b) which is made of PVA film in the UBF. The wavelength range in which the PVA achromatic waveplates are available is from 4000 Å to 7000 Å. The maximum relative error of the retardation is less than 3.00% and the maximum variation of the optical axis is less than $\pm 20'$. The design of the high quality PVA achromatic waveplates is shown in Figures 4(a) and 4(b). The designed parameters and the tested retardations of the PVA achromatic waveplates are listed in Tables IV(a) and IV(b).

2.3. METHOD AND SOME RESULTS OF TESTING THE UBF

To make the passband of the UBF exactly on solar Fraunhofer lines, it is required for the UBF to be tested with a spectrograph. Firstly we find a Fraunhofer line and fix its position on the screen of the monitor, and then put the filter in front of the slit (let the filter be as parallel to the incident light as possible, otherwise the angle of view of the incident light is too big to obtain correct results!). If a horizontal polarizer is put in front of the second thickest element, we can rotate every rotator to put the maxima of the profiles of the crystal elements at an identical position on the screen, and then shift the passband of the filter to the position of the Fraunhofer line by measuring the distance between the two positions. For example, if the passband width of the thickest element on the screen of the monitor is x mm and the distance between the passband and the Fraunhofer line is y mm, the rotating angles and the steps of motors are obtained according to Equation (2.1):

- the second element (No. 1): $\phi_1 = (y/2x) \times \pi$, $s_1 = (y/2x) \times 7560$;
- the first element (No. 2): $\phi_2 = (y/x) \times \pi + \phi_1$, $s_2 = (y/x) \times 7560 + s_1$;

  $\vdots$

- the seventh element (No. 7): $\phi_7 = (y/2^6x) \times \pi + \phi_6$, $s_7 = (y/2^6x) \times 7560 + s_6$.

If the steps of the motors consist of some integer multiples of a period (7560 steps), one can eliminate them to save the rotating time and obtain a number of steps which is less than 7560.

Ten Fraunhofer lines were tested with the method above. The steps of the 7 motors corresponding to the line centers are labelled in Table IV. In order to tune the passband to the required line, one can first get the motors back to the 'zero' position, and then rotate the steps in Table V.

TABLE V

The steps of the 7 motors in the UBF for 10 Fraunhofer lines

Fraunhofer line	No. 1	No. 2	No. 3	No. 4	No. 5	No. 6	No. 7
6562.808 Å	−4727	−2358	−5552	−2076	−1158	−756	−1626
6302.505 Å	−6158	−1480	−1942	−4006	−6386	−7306	−4794
6102.722 Å	−5876	−1634	−2426	−4532	−7192	−546	−5888
5875.743 Å	−7140	−7455	−1844	−3712	−6950	−426	−5424
5576.097 Å	−1144	−5081	−4370	−4480	−7290	−398	−955
5324.185 Å	−2024	−4077	−1321	−3117	−4070	−7080	−1347
5250.212 Å	−7227	−6406	−2814	−3548	−3894	−6842	−1214
5172.699 Å	−6387	−3780	−3260	−1892	−5614	−2162	−672
4861.332 Å	−167	−3182	−736	−5060	−1668	−5543	−7433
4685.682 Å	−4312	−2182	−5991	−1471	−1492	−3300	−7434

TABLE VI

The steps of the motors in the front part of the UBF

Motor number	Optical component	Steps of the motors
8	0° polarizer	−430
	Hollow position	−7427
9	0° polarizer	−53
	Hollow position	−7209
10	0° calibration $\lambda/4$	−5791
	1st hollow position	−14203
	45° calibration $\lambda/4$	−22595
11	5324 Å interference filter	−100
	6563 Å interference filter	−13600

The steps corresponding to the correct positions of the front part, which consists of interference filters, polarizers, calibration quarter achromatic waveplates, are labelled in Table VI.

Some passband profiles of the UBF neighboring the Fraunhofer lines are described in Figure 3.

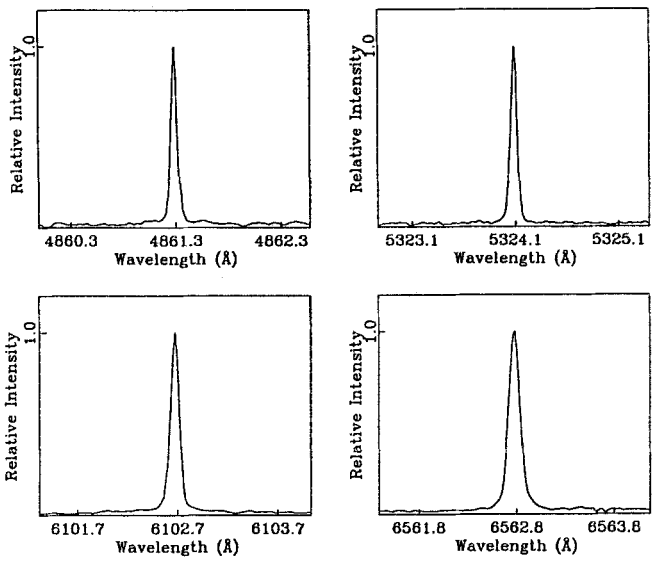

Fig. 3. Some passband profiles of the UBF.

3. The Principles of Magnetic Field and Velocity Field Measurement

3.1. THE NEW DOUBLE PASSBAND MODE

A double passband mode was proposed by Ramsey for a birefringent filter used for a solar video magnetograph (Ramsey, 1971). In this mode, the thickest element is placed in the fore part of the filter and the input polarizer is removed. In the design of the UBF described in this article, a new double passband mode is used in which the second thickest element takes place of the thickest element in Ramsey mode and the thickest element is placed in the middle part of the filter (Figure 1). The new double passband mode has the outstanding merit that the output light intensity is more than twice that of the single passband mode as well as in the Ramsey mode. Compared with the Ramsey mode, the new double passband mode has some other advanced characteristics (Ai, Fear, and Ji, 1990): (1) The two main peaks are placed separately at corresponding wings of the line and the sub-maximum in the opposite wing is much less than that in Ramsey mode, thus giving a higher sensitivity. (2) The temperature drift of the thickest element is reduced.

3.2. MEASUREMENT OF THE MAGNETIC FIELD

In a filter element, the two polarizers may be parallel or perpendicular to each other (see Figure 4):

when $P_1 \| P_2$,

$$\tau_{\|} = \cos^2\left(\frac{\mu d}{\lambda}\pi\right) ; \tag{3.1}$$

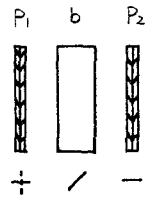

Fig. 4. Two ways of the polarizer orientation in a birefringent filter.

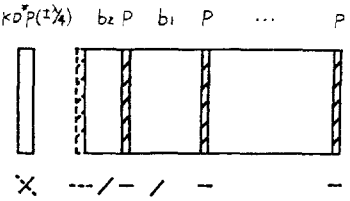

Fig. 5. The optical state of measuring a longitudinal magnetic field.

when $P_1 \perp P_2$,

$$\tau_\perp = \sin^2\left(\frac{\mu d}{\lambda}\pi\right) . \tag{3.2}$$

where μ is the index of birefringence, and d is the thickness of the crystal element. Because $\tau_{\|} + \tau_\perp = 1$, they compensate each other, and the wavelength difference between their main peaks is half a passband.

Left and right circularly polarized light will become mutually orthogonal linear polarized light when passing through a quarter waveplate:

(1) passing through a $+\lambda/4(+45°)$:
left circular light $\rightarrow\leftrightarrow$ (linear),
right circular light $\rightarrow\updownarrow$ (linear);
(2) passing through a $-\lambda/4(-45°)$:
left circular light $\rightarrow\updownarrow$ (linear),
right circular light $\rightarrow\leftrightarrow$ (linear).

According to the Zeeman effect, the light is split into two opposite circularly polarized beams in a longitudinal magnetic field. To study the Zeeman splitting, one can tune the thickest element half a passband and the second thickest element a quarter passband to the wing of a Fraunhofer line which exhibits a strong Zeeman splitting (the optical state as in Figure 5). The profiles of the second thickest and thickest elements are in Figures 6(a) and 6(b). By means of the KD^*P modulator $(\pm\lambda/4)$, the left circularly polarized beam becomes horizontally (0°) and vertically (90°) linear, and the right circular polarized beam becomes vertically (90°) and horizontally (0°) linear simultaneously.

When the KD^*P is $+\lambda/4$, the left and right circularly polarized beams are both passed (Figure 6(c)), and the intensities of them on the CCD camera are I_A, $I_{A'}$,

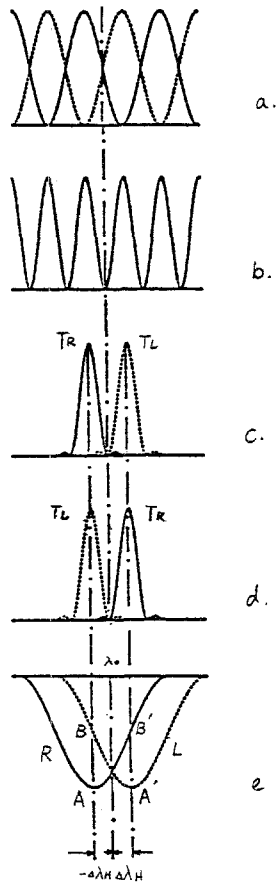

Fig. 6. The principle of measuring a magnetic field. (a) The transmission profiles of the second thickest element when KD^*P is $+\lambda/4$ (solid line) or $-\lambda/4$ (dashed line). (b) The transmission profiles of the thickest element. (c) The transmission profiles of the UBF when the KD^*P is $+\lambda/4$. (d) The transmission profiles of the UBF when KD^*P is $-\lambda/4$. (e) The filter transmission gives the left and right beams different intensities if $\Delta\lambda_H \neq 0$, and $\Delta\lambda_H$ is proportional to the intensity differences.

respectively. When KD^*P is $-\lambda/4$, they are also passed (Figure 6(d)), and the intensities of them on the CCD camera are I_B, $I_{B'}$, respectively. Then the intensity difference is

$$\Delta I_H = (I_B + I_{B'}) - (I_A + I_{A'}) = (I_B - I_A) + (I_{B'} - I_{A'}) = 2(I_B - I_A)\,. \tag{3.3}$$

If $\Delta\lambda_H = 0$, $I_A = I_B$, then $\Delta I_H = 0$. If $\Delta\lambda_H \neq 0$ and small, $\Delta I_H \sim \Delta\lambda_H \sim H$, the longitudinal magnetic field intensity $H(x, y)$ can be obtained.

When a 0° or 45° quarter-wave plate is put in front of the KD^*P modulator, the Q or U component of the vector magnetic field can be obtained.

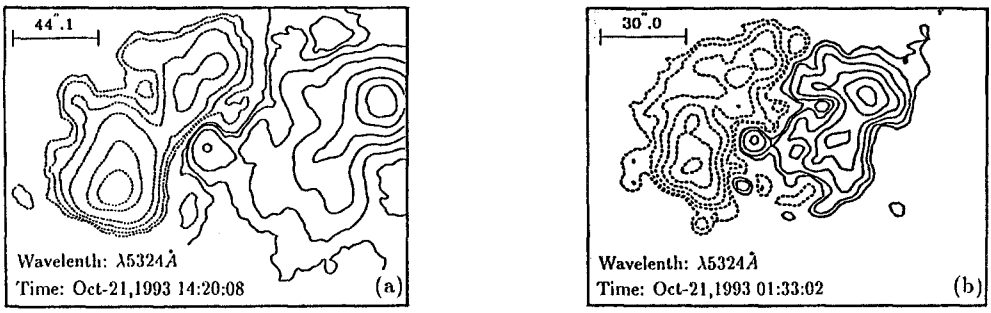

Fig. 7. (a) A magnetograph obtained from the UBF. (b) The corresponding magnetogram obtained from the SMFT. Solid (dashed) contour means north (south) polarity. The calibration grades are ±20, 40, 80, 160, 320, 640, 1280, 1600, 1920, 2240, 2560, 1880 G. Top is north, and west is to the right.

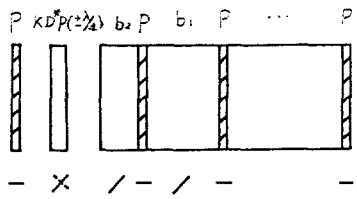

Fig. 8. The optical state for measuring the velocity field.

Figure 7(a) is a line-of-sight magnetogram in Fe λ5324.19 Å obtained from the UBF. Figure 7(b) is the corresponding magnetogram obtained from the Solar Magnetic Field Telescope (SMFT) in Huairou Station, Beijing Astronomical Observatory. From Figures 7(a) and 7(b), the data of the longitudinal magnetic field are identically good in shapes and contour levels. We believe that some differences in the two figures were caused mainly by seeing because there were clouds that day.

3.3. THE MEASUREMENT OF THE LINE-OF-SIGHT VELOCITY FIELD

According to the Doppler effect, the wavelength of the light will be shifted when the source leaves from or approaches the observer. To study Doppler shifting, one can tune the thickest element half a passband to the wing of a Fraunhofer line (the optical state of the filter as in Figure 8). When the KD^*P is $\pm\lambda/4$, the profiles of the filter are A or B (Figure 9). The intensities on the CCD camera are I_A and I_B when the KD^*P is $+\lambda/4$ and $-\lambda/4$, respectively. The intensity difference is

$$\Delta I_V = I_B - I_A \,. \tag{3.4}$$

If $\Delta\lambda_V = 0$, $\Delta I_V = 0$, and if $\Delta\lambda_V \neq 0$ and small, $\Delta I_V \sim \Delta\lambda_V \sim V$, the velocity $V(x, y)$ can be obtained.

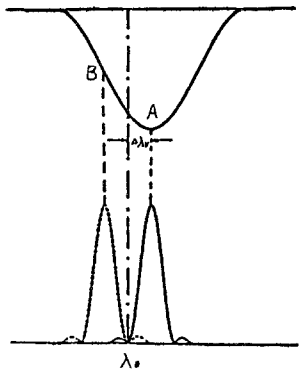

Fig. 9. The filter transmission gives the left and right beams different intensities if $\Delta\lambda_V \neq 0$, and $\Delta\lambda_V$ is proportional to the intensity differences.

4. Conclusion

This universal birefringent filter was built and tested using a spectral telescope in Huairou Station, Beijing Astronomical Observatory in 1993, and then sent to Taiwan Central University. The results of the testing indicate that the UBF with the new double passband mode works well enough for observing chromatic images, measuring vector magnetic fields or line-of-sight velocity fields on the Sun.

The detailed description and the data analysis of the UBF after its regular operation in Taiwan will be published in the future.

Acknowledgements

This research was supported by the Chinese Academy of Sciences and National Science Foundation of China.

References

Ai, G. and Hu, Y.: 1986, *Scientia Sinica* **A7**, 889.
Ai, G., Fear, R. J., and Ji, P.: 1990, *Acta Astrophys. Sinica* **10**, 180.
Evans, J. W.: 1949, *J. Opt. Soc. Amer.* **39**, 229.
Lyot, B.: 1944, *Ann. Astrophys.* **7**, 31.
Panchatnam, S.: 1955, *Proc. Indian Acad. Sci.* **A41**, 130, 137.
Ramsey,H. E.: 1971, *Solar Phys.* **21**, 54.
Šolc, I.: 1949, *J. Opt. Soc. Amer.* **39**, 612.
Title, A.M.: 1976, *Applied Opt.* **15**, 2871.
Wang, J. S., Ai, G., and Deng, Y.: 1991, *Acta Astrophys. Sinica* **11**, 383.